Buitrago, M.; Bertolesi, E.; Calderón García, PA.; Adam, JM. (2021). Robustness of steel truss bridges: laboratory testing of a full-scale 21-metre bridge span. Structures. 29:691-700. https://doi.org/10.1016/j.istruc.2020.12.005

Robustness of steel truss bridges: laboratory testing of a full-scale 21-metre bridge span

Manuel Buitrago[a], Elisa Bertolesi[a], Pedro A. Calderón[a,b] and José M. Adam[a,b*]

[a]*ICITECH, Universitat Politècnica de València. Camino de Vera s/n, 46022 Valencia, Spain*

[b]*CALSENS, Cálculo y Estructuras Sensadas S.L., 46022 Valencia, Spain*

* Corresponding author. Tel.: +34 963877562; fax: +34 963877568.
E-mail address: joadmar@upv.es (José M. Adam).

Abstract

This study aimed to experimentally analyse the robustness of riveted steel bridges based on truss-type structures and to define practical recommendations for early detection of local failures before they cause progressive structural collapse. Although there are many experimental studies on robustness and progressive collapse on buildings, those on bridges are either theoretical or deal with actual collapses. This paper describes a unique case of a 21m full-scale bridge span tested under laboratory conditions with an extensive monitoring system, together with an experimental study to evaluate structural behaviour and robustness as damage or failure progressed in its elements. A linear-static finite-element analysis was also included to examine other possible causes not included in the experiment. The results proved the structural redundancy of this type of truss structure based on the joints' resistance to bending moments and gave rise to a series of practical structural health recommendations to identify early failures and avoid progressive or sudden bridge collapse. The study carried out and the recommendations it produced are now being applied in three similar bridge case studies.

Keywords: *robustness; experimental test; structural health monitoring; progressive collapse; steel truss bridges; riveted joints.*

1. Introduction

Bridge structures are expected to withstand loads defined in codes (e.g. gravity, wind, snow, etc.); however, these structures may be subjected to extreme events (also called low-probability/high-consequence events) such as hurricanes, tsunamis, explosions, vehicle impacts, fires, human errors, terrorist attacks [1,2]; or to be exposed to several degradation actions such as corrosion [3] or fatigue [4]. These events can cause the sudden loss of local elements and trigger a cascading failure of the bridge, known as progressive bridge collapse [5].

Some progressive collapse events gained significant public attention due to the extent of damage and number of victims, as for example: the classic Ronan Point in 1968 [6] or the Twin Towers of the World Trade Center in 2001 [7] in buildings, and the I-35 W bridge in Minnesota [8], the Hongqi Viaduct [9] or Ponte Morandi [10] in bridges. The concept of robustness is introduced in present-day design standards to minimise the risk of progressive collapse. According to this concept, although the risk of local failure cannot be neglected, the aim is rather to control its consequences. Robustness can be generally defined as a measure of the ability of a system to remain functional in the event of a local failure in a single component or a series of connected components [11].

Progressive structural collapse is now a hot topic subjected to widespread theoretical and experimental studies on buildings [12–18]. In bridges, the studies focused basically on the numerical or analytical assessment of robustness (e.g. Ghali and Tadros [1], Wang and Zhou [19], Jiang et al. [20]) or the analysis of real cases (e.g. Starossek [5], Bontempi [7], Deng et al. [8]), including truss bridges [21–29] with an unique experimental test [29]. In truss bridges, from a theoretical viewpoint [21,23,27], it has been shown that a failure in any element can trigger partial or total bridge collapse, so that there is a need for further experimental studies to analyse the real behaviour of these bridges to serve as the basis of future theoretical and numerical developments.

This paper describes the research team's unique opportunity to study a full-scale steel-riveted truss bridge with the double aim of: 1) an experimental analysis of its robustness, and 2) establish practical recommendations for early detection of local failures, which can also set off a progressive collapse. The study was both ambitious and novel and permitted an advance in two areas, including i) the analysis of robustness in the local failure of some elements and ii) structural health monitoring to prevent progressive collapse.

To comply with these aims, after this section a brief description of the bridge is given in Section 2, the test is described in Section, 3 including the transport of the span to the laboratory, the test set-up, procedures and instrumentation used. The experimental results are discussed in Section 4 and are amplified in Section 5 with the aid of computational models. The knowledge obtained from the experimental and theoretical studies was used as the basis for a series of recommendations for early detection of local failures in elements (Section 6) and conclusions are given in Section 7.

2. Description of the bridge

The railway bridge studied was built between 1913 and 1915 and so was more than 100 years old. Its structure was formed by a series of Pratt type trusses connected by riveted joints. It also had a series of horizontal and vertical braces in the form of St. Andrew's crosses, and longitudinal and transverse beams to locally distribute train loads to the Pratt trusses. The heights of the metal piers varied up to 23.6m, and it had two isostatic spans at each end (span length ranged from 21.1m to 21.5m) with a continuous beam in the two central spans (42.0m each). All the supports were hinged with free rotations. One support in each span also had free longitudinal displacement as a roller (A1 for span 1, P1 for span 2, P2 for span 3, P4 for span 4, P5 for span 5 and A2 for span 6). Fig. 1 gives the principal bridge dimensions and a view of a train passing over it.

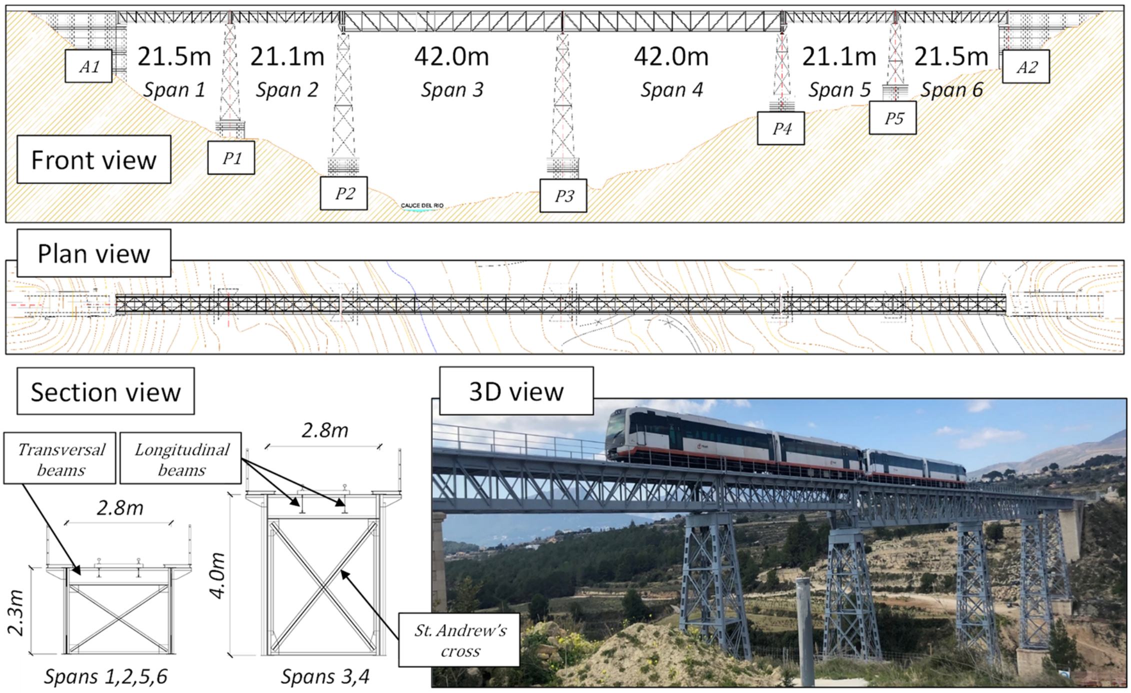

Figure 1. Geometry of the bridge and general views.

(a) Bridge on the railway company's depot

(b) Positioning of the bridge into the ICITECH laboratories

Figure 2. Transport and reception into the ICITECH laboratories.

3. Experimental test

3.1. General

The study was carried out on one of the isostatic spans of a twin of the bridge shown in Fig. 1 with the same geometry and year of construction as the one analysed here and had been in service for the same length of time. The span under consideration had the same characteristics as spans 2 or 5 shown in Fig. 1. It had previously been replaced by a new bridge and was stored at the railway company's depot. This gave to this study a unique opportunity to test a full-scale bridge at the ICITECH laboratories at the *Universitat Politècnica de València* and transfer the results obtained directly to the bridge under study and to others with the same characteristics. Fig. 2(a)-(b) contains a series of photos that illustrate the complex process of transporting the bridge to the ICITECH laboratories.

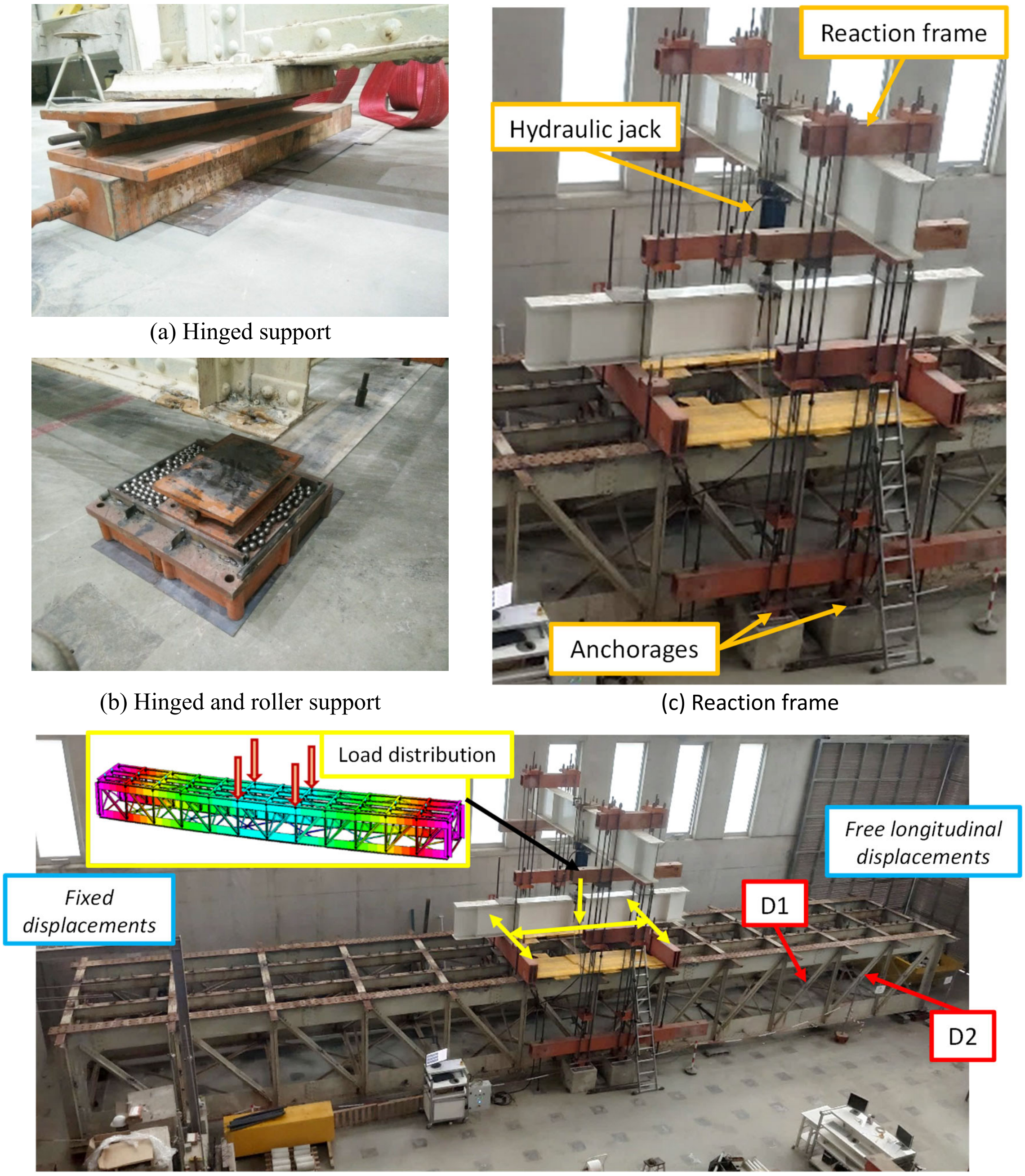

(a) Hinged support

(b) Hinged and roller support

(c) Reaction frame

(d) General view

Figure 3. Test set-up.

3.2. Test set-up

The 21.1m span had the same support conditions as the originals, with free rotations at both sides and longitudinal displacements on one side only. The supports were reproduced in the laboratory with the help of hinges that allowed free longitudinal rotation and a guided box of steel ball-bearings that allowed longitudinal displacement only in the corresponding supports (See Fig. 3(a)-(b), respectively).

The hydraulic jack with a maximum load capacity of 1300kN used to test the bridge was installed with the help of a reaction frame at the centre of the span which was anchored to the laboratory's reaction slab. The load applied by the jack was shared between 4 points by a system of metal girders to avoid high load concentrations. The test setup and details of the load distribution system can be seen in Fig. 3(c)-(d).

3.3. Sequence of damage and load

Two types of very different approaches can be used to study structural robustness in sudden failures: the scenario-dependent [30] and scenario-independent [13]. The first is used to study and consider the cause of the failure while the second only aims to minimize the consequences, whatever the cause. Both have the common aim of improving robustness by studying the behaviour in sudden local failures in a component. In the present experimental study the scenario-independent approach was selected to: a) analyse structural robustness after a series of damage to some elements, b) study the structural behaviour after activating Alternative Load Paths (ALPs), and c) establish a number of directives in order to anticipate structural failures that could end in total collapse.

To achieve these objectives a structural damage sequence was designed to analyse behaviour with the evolution of deliberately caused damage. In the test the damage was only caused in the diagonals that had previously been expected to provide effectively activated ALPs. Other more complicated cases such as main chord failure were analysed numerically (see Section 5).

The diagonals selected to reproduce progressive damage with possible sudden collapse were those labelled D1 and D2 in Fig. 3(d) and were chosen as being the most critical both in the test carried out and in actual service. The load on these diagonals was lower than that on the external diagonal, although strains and stresses were higher due to being smaller sections. Fig. 4 shows the sequence of the damage in the test, in which the shaded section represents the break made to simulate damage evolution. After each damage sequence a load increment of up to 1250kN was gradually applied with a force-controlled mode and the structural response was determined by the ambitious monitoring system described below.

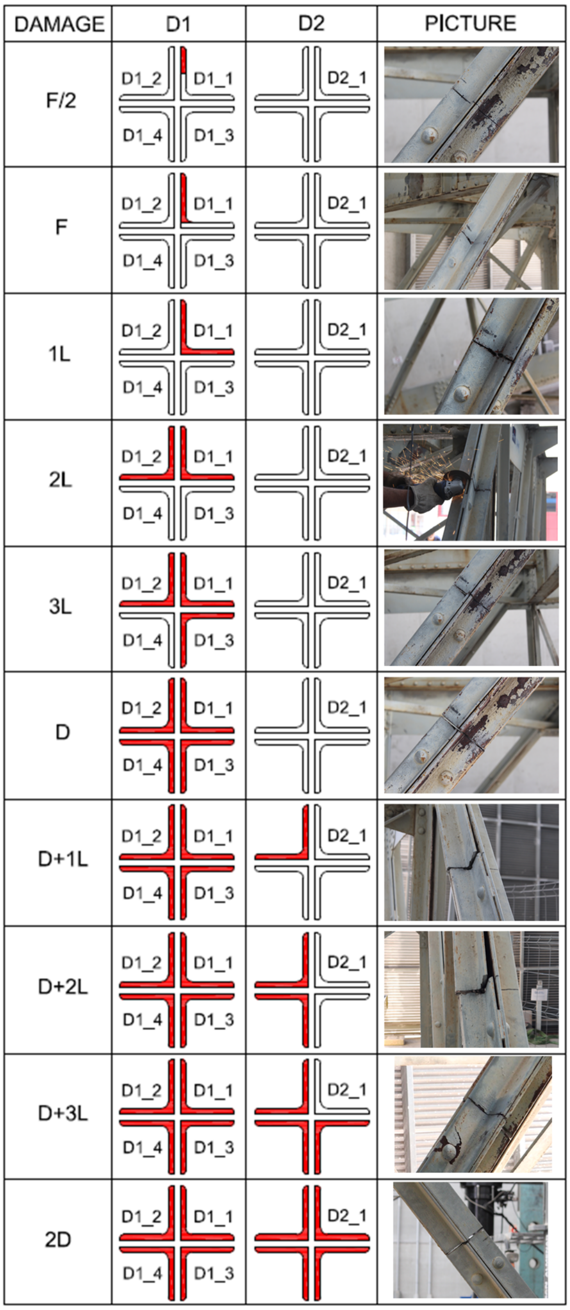

Figure 4. Sequence of damage.

3.4. Instrumentation

The monitoring equipment consisted of 40 strain gauges (SG in Fig. 5), 8 LVDTs (D, L and T in Fig. 5) and 2 fibre optic accelerometers (A in Fig. 5).

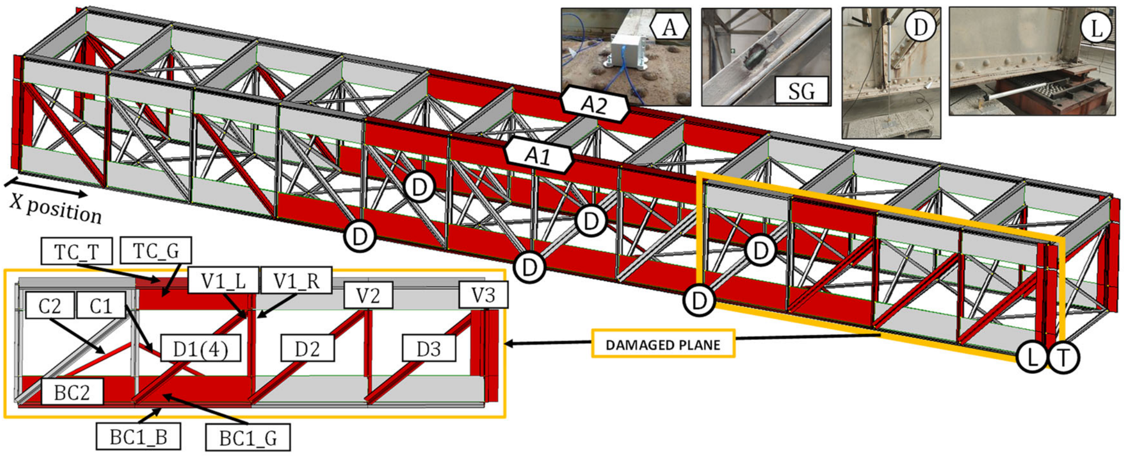

Figure 5. Instrumentation.

The 40 strain gauges were located in different positions on the bridge to analyse the structural response at each damage level (see red elements in Fig. 5). The most important for the study are depicted in Fig. 5. In general, each element only had one strain gauge at the centre of gravity and in the middle of the length. However, diagonal D1 with 4 strain gauges, and vertical column V1 and top (TC) and bottom (BC1) chords with 2 strain gauges each were more intensively monitored, as can be seen in Figs. 4-5. The sensors for D1 were installed on the L-profiles of the diagonal, at mid-length (see Fig. 4). In the case of V1 (see Fig. 5), the sensors were installed on the upper left (V1-L) and right (V1-R) where modifications of the deformations were expected as damage intensified (see Section 4 and 5 for further details). The two sensors at V1 were installed just before the test for level 3L damage. For the top and bottom chords (see Fig. 5) they were placed on the external surface (TC_T and BC1_B) and at the centre of gravity of the elements (TC-G and BC1_G).

LVDTs measured bridge deflection (D) and longitudinal displacement (L) in the mobile support during the test. For safety reasons possible sideways displacements were also controlled (T) (see Fig. 5).

The accelerometers were placed at the mid-span (see Fig. 5) to measure the eigenfrequency of the first vertical vibration mode. The value was determined by measuring acceleration after an impact at mid-span after the test at each damage level.

4. Test results. Analysis and discussion

4.1. Strain gauges

Fig. 6 shows the stresses obtained in diagonals from the readings of strain gauges after each damage level. The stresses are seen to decline as the breaks were made in diagonal D1, except in sensor D1_4 belonging to the last damaged L-profile. The reduction of the diagonal D1 cross-section by the previous breaks increased the stresses by up to 53% the L-profile monitored by sensor D1_4.

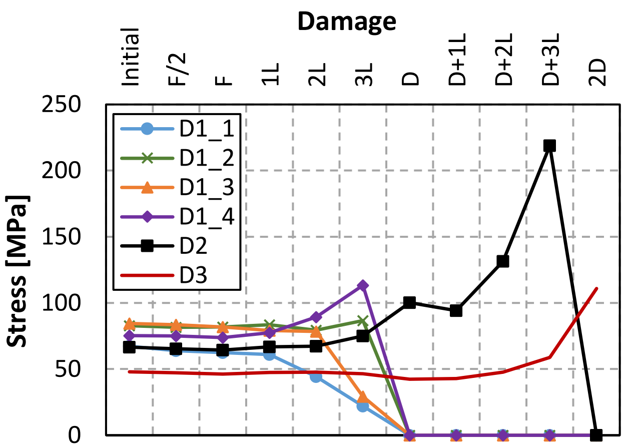

Figure 6. Stresses in diagonals D1, D2 and D3.

Up to the complete break of the first diagonal (level of damage D; see Fig. 6), the sensors on D2 and D3 did not show any significant changes. The stresses only increased in diagonal D2 after damage 3L but this was not really significant until D1 was completely broken (damage level D) and breaks began to be made in D2, which subsequently suffered much higher stresses of up to 240%. D3 did not register a significant stress increase (up to 136%) until three L-profiles in diagonal D2 were broken (damage level D+3L). This shows that the diagonals beside the damaged one do not experience significantly higher loads until the area of the damaged one has been reduced by 75%, which indicates: a) the shear distribution in the Pratt truss remains similar until a diagonal has been completely broken, and b) ALPs must be activated on complete breakage of a diagonal (damage level D and 2D) (analysed in detail below), which significantly raises the loads on the neighbouring diagonals. This load increase on these diagonals cannot be explained simply by the different load distribution theoretically expected for a Pratt truss since the shear of the span did not change (it is important to note that truss elements usually work only under axial loads to transmit the shear and bending moments of the span to the supports).

Fig. 7 shows the stresses obtained for each damage level in the tests in vertical column V1 and crosses C1 and C2. The results for V1 confirm the activation of ALPs after complete failure of a diagonal, with significant higher stresses at damage levels D and 2D. The vertical column starts mainly from compression plus small bending and finishes with serious bending plus compression, sensor V1_L being in compression and V1_R in tension. However, sensor V2 (and V3, not shown in Fig. 7), which was installed at mid-height of the vertical column, was not able to measure any significant change due to the insignificant bending in the middle of the vertical columns. The analysis thus shows that: a) damage to the diagonals can only be registered by sensors at the ends of vertical columns, and b) the highest absolute stress values were recorded in the compressed part of these elements, which improved the sensors' accuracy.

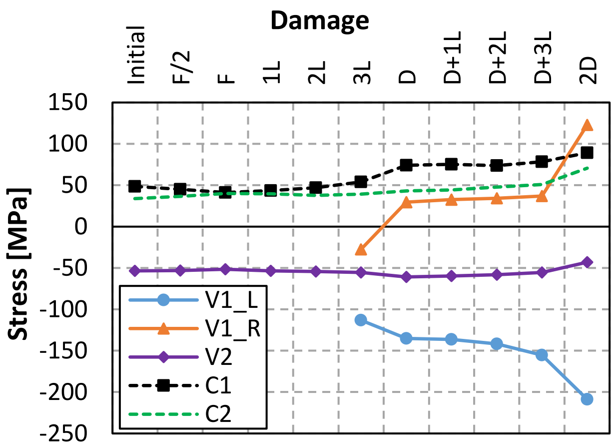

Figure 7. Stresses in vertical columns V1 and V2 and horizontal crosses C1 and C2.

Crosses C1 and C2 were also affected by the damage (see Fig. 7). Although stress increments were not as significant as those in the vertical columns, cross C1, which was closer to the damage, also registered a stress increment up to 85%. This increment means that the structure was trying to reduce the distortion caused by a more flexible Pratt truss (in the damaged plane) to the overall structure than the more rigid Pratt truss on the undamaged plane.

Fig. 8 shows the stresses obtained in the tests after each damage level in bottom (BC1_B and BC1_G) and top (TC_G and TC_T) chords. The sensors detected a marked rise of the bending moment in both chords, with lower measured values at the centre of gravity (G) than those measured at the external part of the element (B and T for bottom and top chord, respectively). This shows that: a) bending was induced in the chords by the damage, b) the biggest stress change were at the ends of the chords due to the stronger bending effect. It is important to remember here that the sensors, as shown in Fig. 5, were placed close to a joint and not at the element's mid-length (a more detailed discussion can be found in Section 5). The sensor on bottom chord BC2 (not shown in Fig. 8), which was installed at its centre of gravity and mid-length did not register any significant change during the test.

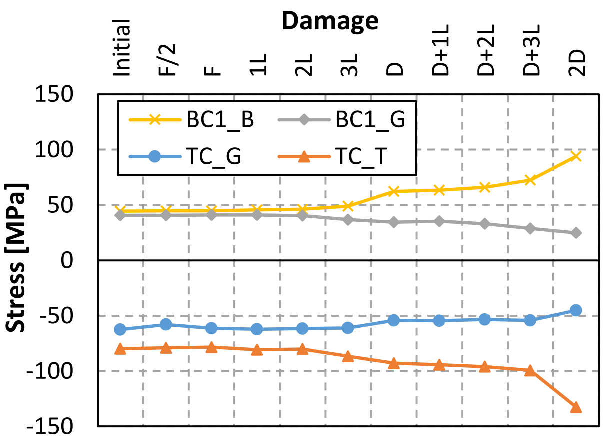

Figure 8. Stresses in top (TC_T and TC_G) and bottom (BC1_B, BC1_G and BC2) chords.

4.2. Deflections

Fig. 9 shows the deformed shape of the damaged and the undamaged Pratt truss (damaged and undamaged plane, respectively) during the damage and test sequence. The behaviour of both trusses is markedly different. Deflections measured on the undamaged truss were not affected by the damage sequence with a maximum vertical deflection at mid-span slightly over 25mm.

However, deflections on the damaged plane were strongly affected by the damage sequence, starting with the same deflection (25mm) and ending with 40mm deflection at mid-span. Measuring deflections on the damaged plane can thus be considered an effective way of interpreting damage by registering significant changes in both the maximum value and deformed shape, which was greater on the right (position X between 10.6m and 21.1m).

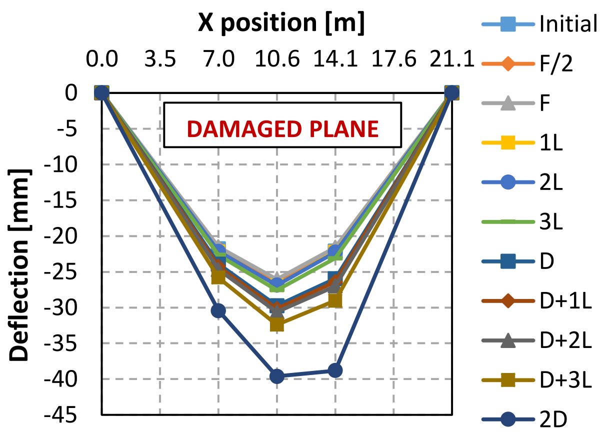

(a) Damaged plane

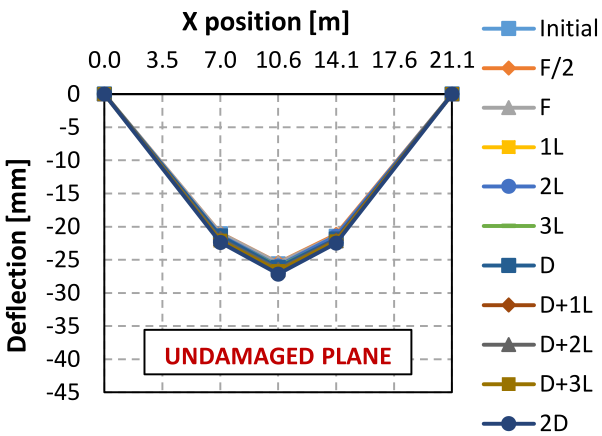

(b) Undamaged plane

Figure 9. Evolution of deflections.

4.3. Horizontal displacements

As horizontal displacements remained small during the different test damage levels, with a maximum of 5mm for the longitudinal one, they could not be regarded as a reliable indicator of structural damage. Transversal displacement stayed close to 0 and confirmed that the supports installed for the tests worked well.

4.4. Vibrational modes

The accelerometers A1 (in the damaged Pratt truss) and A2 (in the undamaged Pratt truss) installed at mid-span gave the eigenfrequencies of the structure's first vertical vibration mode. Fig. 10 gives the results obtained together with the accelerometer A1 trend line. It can be seen that the first vertical vibration mode falls as damage is increased and the reduced frequency levels are similar for both A1 and A2.

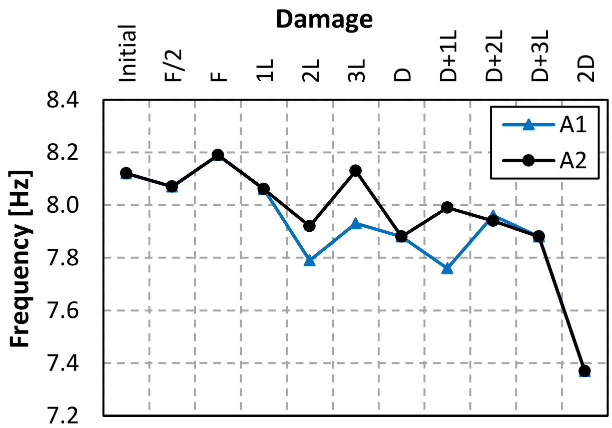

Figure 10. Evolution of the first vibration mode.

4.5. Discussion

The span under study consisted of Pratt trusses considered as externally and internally isostatic working under axial forces only. Consulting companies usually consider these types as structures of truss elements with hinges at the ends. If this had been true the present study would not have been possible since it would have lacked structural redundancy. However, the structure was shown to have the ability to adapt to the total failure of key elements such as diagonals.

This adaptability was possible thanks to the effective activation of ALPs. In this case the structure, which worked basically under axial forces, made use of the structural redundancy of the joints to adapt to the failure of diagonals, as the joints were able to resist high bending moments. Thanks to this ability, when the diagonals failed, the structural behaviour of the affected zone changed from Pratt truss to Vierendeel behaviour (same structure but without diagonals; see Fig. 11), in which the capacity of the joints to resist bending moments is crucial. When a structure like the span under study has no diagonals, the structure is known as a Vierendeel beam, and the load transmission to the foundations is only possible with the help of the moment-resisting capacity of joints. The moments registered in the vertical columns and top and bottom chords (see Section 4.1) confirm this hypothesis (see also Section 5).

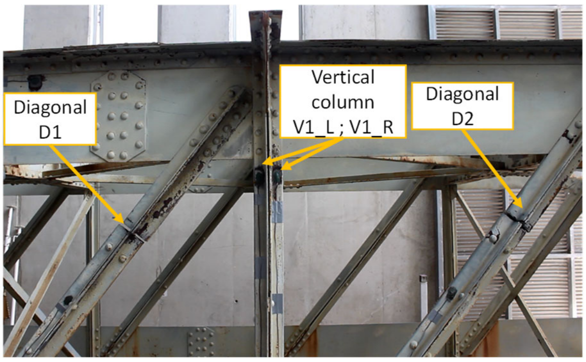

Figure 11. Deformed shape during the test after level of damage 2D.

5. Finite Element Modelling

A Finite Element Analysis (FEA) [31] could be used to analyse other failures not considered in the experiment. The FE model reproduced the bridge geometry through BEAM elements fully connected and with a combination of BEAM and SHELL elements for the top and bottom chords to fit the numerical results better to the actual structural behaviour (steel elastic modulus of 210GPa and density equal to 78.5kN/m^3). The boundary conditions applied were identical to those in the test with fixed displacements and free rotations in the four supports. The supports at X = 21.1m also had free longitudinal displacements. Fig. 12 shows the FE model of the bridge span.

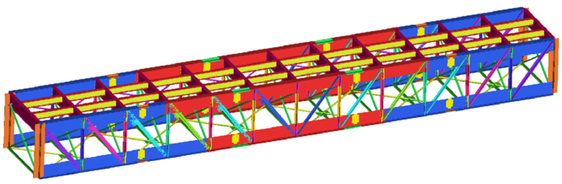

Figure 12. FE model.

5.1. Reproduction of the test failure schemes

Firstly, a modal analysis was carried out to compare the frequency of the first vertical vibrational mode of the original structure and the structure without diagonals D1 and D2 with the experimental results. Table 1 gives the numerical and experimental results obtained and the frequency reduction in both cases for damage levels D and 2D. The numerical results can be seen to reproduce the experimental results, with similar frequency reduction percentages to those obtained in the test.

Table 1. Comparison of frequencies between numerical and tests results.

		Level of damage		
		Initial	D	2D
Experimental	Frequency [Hz]	8.12	7.88	7.37
	Reduction [%]	---	2.96	9.24
Numerical	Frequency [Hz]	8.72	8.53	7.95
	Reduction [%]	---	2.18	8.83

Secondly, Linear-Static Finite-Element Analyses (LSFEAs) were performed for different damage levels (Initial, D and 2D) considering geometrical nonlinearities. A steel elasticity modulus of 210GPa was considered with the application of a load of 1250kN, as in the test. Fig. 13 shows the deformed shape and stresses of the structure (in the damaged plane) for the different levels. Both deformed shape and stresses are similar to those obtained experimentally. The numerical analysis again shows the activation of ALPs mentioned in Section 4.5, since as damage rose the bending moments also increased considerably causing the different elements (vertical columns and top and bottom chords) to be subjected to high stress gradients in specific sections close to joints (see Fig. 13). This shows that the LSFEA numerical simulation reproduced the experimental behaviour and that the models were properly built. This analysis can thus be extended to failures of other more affected elements not considered in the experiments such as the most heavily loaded bottom chord, which would be extremely difficult to analyse experimentally and safely in a laboratory.

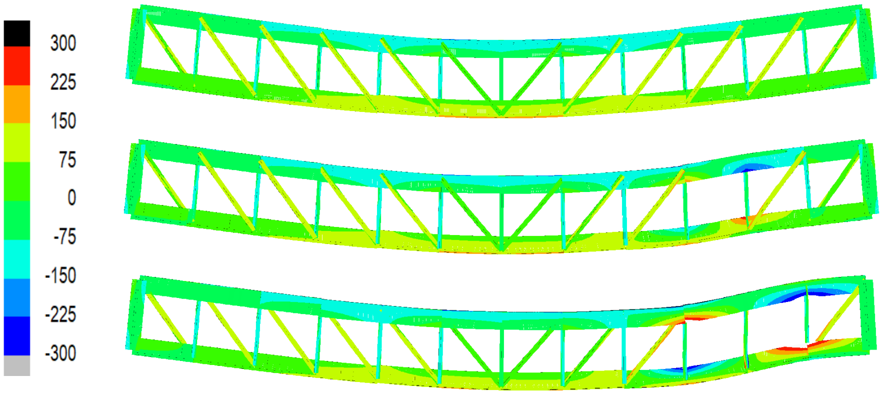

Figure 13. Total stresses for Initial, D and 2D damaged levels. Units: MPa.

5.2. Failure of the most heavily loaded bottom chord

This case was analysed by LSFEAs for two damage levels: 1) a section flange failure and 2) complete section failure (see Fig. 14(b)-(c)). All three cases (initial plus two damage levels) were assessed under the same loading scheme described in the previous sections, with a maximum load of 1250kN.

In the most heavily loaded bottom chord flange failure, small increases were found in the stresses on neighbouring elements, especially those due to higher bending moments, although, like the deformed shape, these increases were not significant. In fact, Figs. 14(a)-(b) do not show any significant differences of structural behaviour, indicating that significant ALP activation was not necessary. The Pratt trusses were able to carry on efficiently working the elements mainly under axial loads. In the natural frequencies, the first vertical vibrational mode frequency changed slightly from 8.72Hz to 8.71Hz.

In the complete section failure of the most heavily loaded bottom chord significant structural behavioural differences were found (see Figs. 14(a)-(c)). The numerically reproduced damage (Fig. 14(c)) was quite severe, eliminated Pratt truss-type behaviour close to the failure, and the top chord was the main element in resisting bending moments and axial and shear forces. There were also stress changes in the elements close to the failure, the deformed shape was also significantly different and the first vertical vibrational mode frequency changed from 8.72Hz to 6.70Hz. In this case the structure did have to find an effective ALP and passed from Pratt truss to a basically Beam-type top chord behaviour in the failure zone. All of the parameters used (stresses, deformed shape, natural frequencies) were good indicators of the computer-simulated failure.

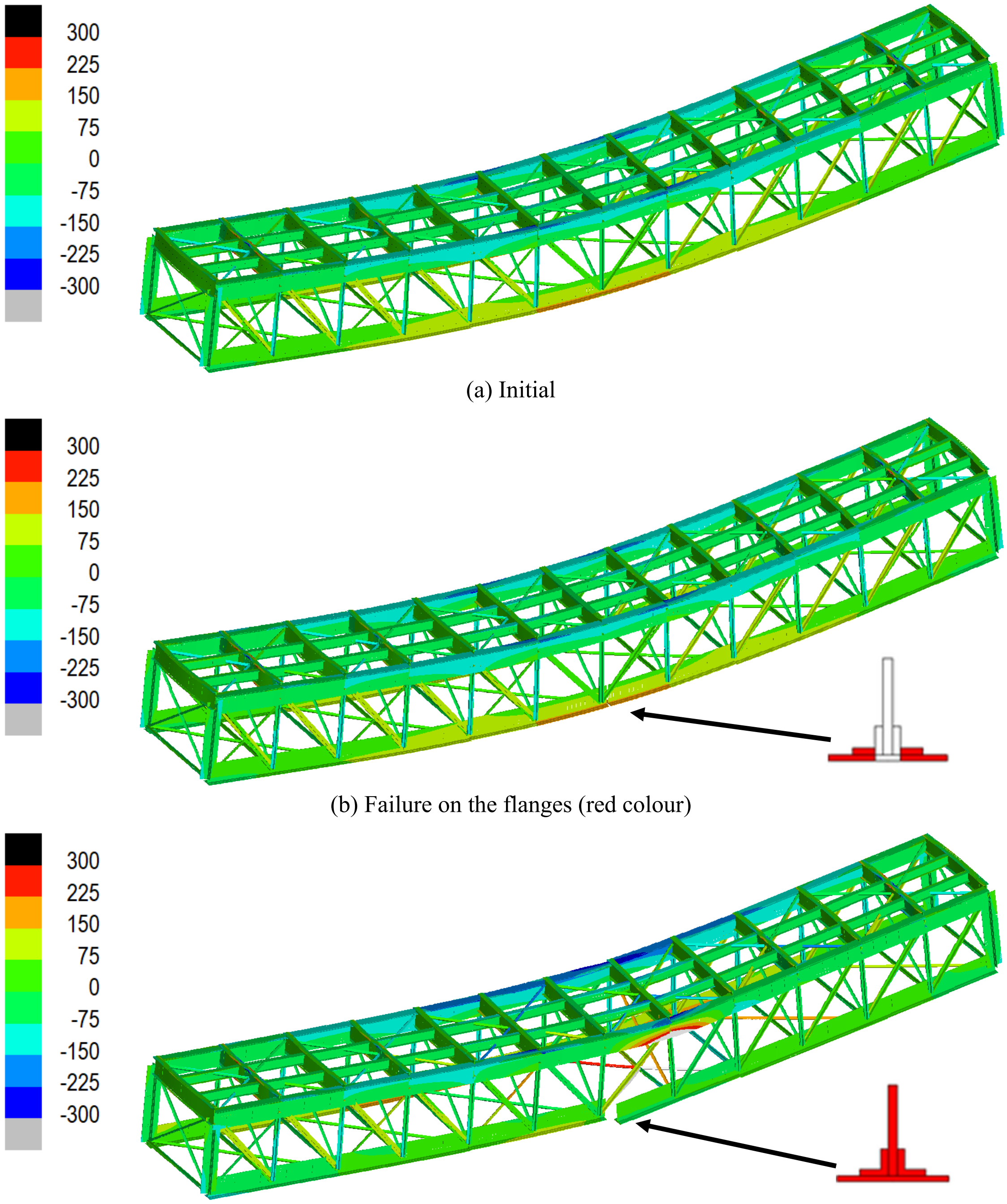

(a) Initial

(b) Failure on the flanges (red colour)

(c) Failure of a complete section (red colour)

Figure 14. Total stresses for the different damage levels in the failure of the most heavily loaded bottom chord. Units: MPa.

6. Practical recommendations for Structural Health Monitoring

Based on the results obtained, this section aims to lay down a series of recommendations for real-time monitoring of structures similar to the type studied here for early failure detection, including aspects such as: a) parameters to be controlled, b) appropriate sensors for different parameters and c) a specific location for each type of sensor.

Firstly, it is recommended to monitor element deformation by strain gauges. As found previously, the breakage or damage progress of an element and its neighbours is reflected by its deformation. It is thus recommended to arrange sensors around the structure on its most critical elements, for example strain gauges in the external diagonals and vertical columns (maximum shear) and chords near the mid-span (maximum bending) both for conventional monitoring (e.g. load tests) and early failure detection. Strain gauges should be installed at the centre of gravity and the centre of the elements to measure axial loads in truss structures (theoretically, elements are only subjected to axial loads in truss structures). However, other sensor locations are recommended to detect early failures, such as away from the section's centre of gravity and closer to the joints instead of at the centre. Besides considering the effect of failure on the axial load on the element at these points, the considerable effects of the bending moments with effective ALPs in action to cover structural failure will also be included. Sensors can also be placed on elements expected to be subjected to higher instead of reduced deformation in order to reduce measurement errors. Table 2 gives a summary of all this information with recommendations for monitoring and early failure detection of the different elements.

Table 2. Location of strain sensors.

Element	General purpose	Early failure detection	
		General position	Additional details. To be measured in case of failure
Chords	Section: Centre of gravity	Section: far from the centre of gravity	Compression and tension increments in the top and bottom chords, respectively
Diagonals			Tension increments
Vertical columns	Position: Centre of the length of the element	Position: close to a joint	Compression increments. In general, in the point of the element closer to the centre of the bay

Secondly, it is recommended to monitor deflections by any of the different methods, for example topography or LVDTs. As in conventional monitoring, it is generally enough to measure deflection at one point at mid-span, although early failure detection may require monitoring deflection at other points (see Fig. 9). Full monitoring can be carried out by measuring deflection at two points at mid-span and at a quarter and three quarters the length of the span (4 extra points) as was done in the test in the present study (see Fig. 5). This is important to identify the site of the failure.

Finally, as can be extracted from the experimental and numerical results, accelerations can also be measured in a bridge to obtain the principal structural vibration modes in real time. All types of structural anomalies can be reflected by small changes in the frequencies of the structure's main vibrational modes. It is recommended to install at least two accelerometers for the control of the first vertical vibrational mode (1 accelerometer at mid-span is sufficient). A more complete system would also include two additional accelerometers in each span, one also in the middle of the span but on the opposite frame to follow the structure's possible torsional mode, with the other at a quarter or three quarters the length of the span to follow the second vertical vibration mode.

All the information obtained from the present study, and its recommendations, are now being applied to three real bridge case studies in an ambitious real-time monitoring system with a system of 350 strain gauges and 46 accelerometers. Deflections are also registered periodically by static load tests. The practical recommendations will be validated further in future studies with the data analysis of the above three case studies.

7. Conclusions

This paper described an experimental study of the robustness of a steel riveted truss bridge on getting the opportunity to lab-test a full-scale bridge span. From this test and the subsequent numerical analysis the following conclusions could be obtained:

- The structure, theoretically with truss-type behaviour had structural redundancy based on the joints' capacity to absorb bending moments that increase with the level of damage.
- During the failure and the evolution of the damage to some of the structural elements it was found that:
    - The stresses on nearby elements were highest at points close to the joints most susceptible to bending moments with increases of up to 240%.
    - There were significant changes in the deformed shape of the structure. Deflections reached 60% increments.
    - The first vertical natural frequency was reduced by up to 9.2%.
- The structure was able to find effective alternative load paths (ALPs) and changed its function from Pratt truss to Vierendeel or single-beam behaviour. These ALPs were limited by the structural load levels until some of the elements initiated plastic behaviour.
- A set of practical recommendations were made for structural health monitoring with the aim of identifying early failures. These recommendations were provided for different parameters (strains, deflections, accelerations), and the type, location and number of sensors for a structure with both a basic and an ambitious monitoring system.

In future work, a further validation of these practical recommendations will be made with the data analysis of three real case studies on different railway bridges in which an ambitious monitoring system with more than 400 sensors was installed.

Acknowledgements

We would like to express our gratitude to the FGV (*Ferrocarrils de la Generalitat Valenciana*) and *FCC Construcción S.A., CHM Obras e Infraestructuras S.A., Contratas y Ventas S.A.* and *CALSENS S.L.* for giving us the opportunity to test a bridge at the ICITECH facilities, also to Juan Antonio García Cerezo, of FGV, for his invaluable cooperation and recommendations. We also wish to show our gratitude for the magnificent work on the bridge by Jesús Martínez, Eduardo Luengo and Daniel Tasquer. The tests on the bridge meant that much of the Structures Laboratory was out of service for other work, for which we owe a debt of gratitude to our ICITECH colleagues for their infinite patience and understanding.

References

[1] Ghali A, Tadros G. Bridge progressive collapse vulnerability. J Struct Eng 1997;123:227–31. doi:10.1061/(ASCE)0733-9445(1997)123:2(227).

[2] Cha EJ, Ellingwood BR. Risk-averse decision-making for civil infrastructure exposed to low-probability, high-consequence events. Reliab Eng Syst Saf 2012;104:27–35. doi:10.1016/J.RESS.2012.04.002.

[3] Colajanni P, Recupero A, Ricciardi G, Spinella N. Failure by corrosion in PC bridges: a case history of a viaduct in Italy. Int J Struct Integr 2016;7:181–93. doi:10.1108/IJSI-09-2014-0046.

[4] Zhuang M, Miao C. Fatigue reliability assessment for hangers of a special-shaped CFST arch bridge. Structures 2020;28:235–50. doi:10.1016/j.istruc.2020.08.067.

[5] Starossek U. Avoiding disproportionate collapse of major bridges. Struct Eng Int 2009;19:289–97. doi:10.2749/101686609788957838.

[6] Russell JM, Sagaseta J, Cormie D, Jones AEK. Historical review of prescriptive design rules for robustness after the collapse of Ronan Point. Structures 2019;20:365–73. doi:10.1016/j.istruc.2019.04.011.

[7] Bontempi F. Elementary concepts of structural robustness of bridges and viaducts. J Civ Struct Heal Monit 2019;9:703–17. doi:10.1007/s13349-019-00362-7.

[8] Deng L, Wang W, Yu Y. State-of-the-Art Review on the Causes and Mechanisms of Bridge Collapse. J Perform Constr Facil 2016;30:04015005.

doi:10.1061/(ASCE)CF.1943-5509.0000731.

[9] Bi K, Ren W-X, Cheng P-F, Hao H. Domino-type progressive collapse analysis of a multi-span simply-supported bridge: A case study. Eng Struct 2015;90:172–82. doi:10.1016/J.ENGSTRUCT.2015.02.023.

[10] Rania N, Coppola I, Martorana F, Migliorini L. The collapse of the Morandi bridge in Genoa on 14 august 2018: a collective traumatic event and its emotional impact linked to the place and loss of a symbol. Sustainability 2019;11:6822. doi:10.3390/su11236822.

[11] Buitrago M, Sagaseta J, Adam JM. Avoiding failures during building construction using structural fuses as load limiters on temporary shoring structures. Eng Struct 2020;204:109906. doi:10.1016/j.engstruct.2019.109906.

[12] Adam JM, Parisi F, Sagaseta J, Lu X. Research and practice on progressive collapse and robustness of building structures in the 21st century. Eng Struct 2018;173:122–49. doi:10.1016/j.engstruct.2018.06.082.

[13] Adam JM, Buitrago M, Bertolesi E, Sagaseta J, Moragues JJ. Dynamic performance of a real-scale reinforced concrete building test under corner-column failure scenario. Eng Struct 2020;210:110414. doi:10.1016/j.engstruct.2020.110414.

[14] Alshaikh IMH, Bakar BHA, Alwesabi EAH, Akil HM. Experimental investigation of the progressive collapse of reinforced concrete structures: An overview. Structures 2020;25:881–900. doi:10.1016/J.ISTRUC.2020.03.018.

[15] Fu Q, Tan K-H. Numerical study on steel-concrete composite floor systems under corner column removal scenario. Structures 2019. doi:10.1016/j.istruc.2019.06.003.

[16] Mucedero G, Brunesi E, Parisi F. Nonlinear material modelling for fibre-based progressive collapse analysis of RC framed buildings. Eng Fail Anal 2020;118:104901. doi:10.1016/j.engfailanal.2020.104901.

[17] Bao Y, Main JA, Noh S-Y. Evaluation of Structural Robustness against Column Loss: Methodology and Application to RC Frame Buildings. J Struct Eng 2017;143:04017066. doi:10.1061/(asce)st.1943-541x.0001795.

[18] Eren N, Brunesi E, Nascimbene R. Influence of masonry infills on the progressive collapse resistance of reinforced concrete framed buildings. Eng Struct 2019;178:375–94. doi:10.1016/J.ENGSTRUCT.2018.10.056.

[19] Wang MR, Zhou ZJ. Progressive collapse and structural robustness of bridges. Appl Mech Mater 2012;193–194:1021–4. doi:10.4028/www.scientific.net/AMM.193-194.1021.

[20] Jiang H, Wang J, Chorzepa MG, Zhao J. Numerical investigation of progressive collapse of a multispan continuous bridge subjected to vessel collision. J Bridg Eng 2017;22:04017008. doi:10.1061/(ASCE)BE.1943-5592.0001037.

[21] Miyachi K, Nakamura S, Manda A. Progressive collapse analysis of steel truss bridges and evaluation of ductility. J Constr Steel Res 2012;78:192–200. doi:10.1016/J.JCSR.2012.06.015.

[22] Garavaglia E, Sgambi L, Basso N. Selective maintenance strategies applied to a bridge deteriorating steel truss. Bridg. Maintenance, Safety, Manag. Resil. Sustain. - Proc. Sixth Int. Conf. Bridg. Maintenance, Saf. Manag., 2012, p. 1764–70. doi:10.1201/b12352-258.

[23] Khuyen HT, Iwasaki E. An approximate method of dynamic amplification factor for alternate load path in redundancy and progressive collapse linear static analysis for steel truss bridges. Case Stud Struct Eng 2016;6:53–62. doi:10.1016/J.CSSE.2016.06.001.

[24] Olmati P, Brando F, Gkoumas K. Robustness assessment of a steel truss bridge. Struct.

Congr., Reston, VA: American Society of Civil Engineers; 2013, p. 250–61. doi:10.1061/9780784412848.023.

[25] Trong Khuyen H, Eiji I. Linear redundancy analysis method considering plastic region for steel truss bridges. J Bridg Eng 2017;22:05016011. doi:10.1061/(ASCE)BE.1943-5592.0000999.

[26] Garavaglia E, Sgambi L. Selective maintenance planning of a steel truss bridge based on the Markovian approach. Eng Struct 2016;125:532–45. doi:10.1016/J.ENGSTRUCT.2016.06.055.

[27] Ma X, Han B. Analysis and mitigation of progressive collapse for steel truss girders. 2011 Second Int. Conf. Mech. Autom. Control Eng., IEEE; 2011, p. 1931–4. doi:10.1109/MACE.2011.5987345.

[28] Olmati P, Gkoumas K, Brando F, Cao L. Consequence-based robustness assessment of a steel truss bridge. Struct. Congr., Techno-Press; 2013, p. 250–61. doi:10.12989/scs.2013.14.4.379.

[29] Azizinamini A. Full scale testing of old steel truss bridge. J Constr Steel Res 2002;58:843–58. doi:10.1016/S0143-974X(01)00096-7.

[30] Sagaseta J, Olmati P, Micallef K, Cormie D. Punching shear failure in blast-loaded RC slabs and panels. Eng Struct 2017;147:177–94. doi:10.1016/j.engstruct.2017.04.051.

[31] ABAQUS v16.4. Abaqus, Theory manual 2016.